Acta Crystallographica Section B
Structural Science
ISSN 0108-7681

Experimental *versus* expected halide-ion size differences; structural changes in three series of isotypic bismuth chalcogenide halides

Egbert Keller* and Volker Krämer

Kristallographisches Institut der Universität Freiburg, Hermann-Herder-Straße 5, D-79104 Freiburg, Germany

Correspondence e-mail: egbert.keller@krist.uni-freiburg.de

Received 28 October 2005
Accepted 13 March 2006

Experimentally determined halide-ion size differences are compared with expected size differences in the three series of isotypic bismuth chalcogenide halide compounds, KBi_6O_9X (X = Cl, Br and I), BiOX (X = F, Cl, Br and I) and BiSX (X = Cl, Br and I). The strong deviations observed can be assigned to steric strain caused by the heterogenity of the bond-valence pattern and (for BiOX) to anion–anion repulsion and a change in the connectivity scheme. Some special features of the BiOF structure and the question of 'isotypism' within the BiOX series are briefly discussed. Structural changes within the BiSX series are analysed.

Dedicated to Professor Heinrich Vahrenkamp, Prof. *emeritus* of the Institut für Anorganische und Analytische Chemie der Albert–Ludwigs–Universität Freiburg.

1. Introduction

Recently we have presented a method to calculate expectation values $\langle\Delta\rho_{XY}\rangle$ for 'ionic' size differences in isotypic structures from bond-valence (BV) parameters and ionic radii (IR); numerous $\langle\Delta\rho_{XY}\rangle$ values for pairs of isovalent main group and transition group element 'ions' have been tabulated (Keller & Krämer, 2006). Theoretically, $\langle\Delta\rho_{XY}\rangle$ is supposed to predict the change in any bond length $E-X$, when X is replaced by Y, provided that the resulting structure is (nearly) isotypic to the one before.

The initial aim of that work was to obtain reliable size differences for the halide ions to be used in a study of the structural changes within three series of bismuth chalcogenide halide compounds. The compounds in question are the isotypic series KBi_6O_9X (X = Cl, Br and I; Eggenweiler *et al.*, 1998), BiOX (X = F, Cl, Br and I; Aurivillius, 1964; Soubeyroux *et al.*, 1984; Keramidas *et al.*, 1993; Ketterer & Krämer, 1986; Keller & Krämer, 2005), and BiSX (X = Cl, Br and I; Voutsas & Rentzeperis, 1980, 1984; Haase-Wessel, 1973). The KBi_6O_9X structure (space group $I\overline{4}3d$) consists of a $\{^3_\infty\}[Bi_2O_3]$ framework penetrated by infinite non-intersecting linear K$-X$ chains parallel to ⟨111⟩ (Fig. 1). BiOX (space group $P4/nmm$) adopts the PbFCl structure, *i.e.* its structure is built from $\{^2_\infty\}[X(Bi_2O_2)X]$ 'sandwich' layers interacting *via* van der Waals forces (Fig. 2). The structure of BiSX (space group *Pnma*) can be described as a packing of $\{^1_\infty\}[X(Bi_2S_2)X]$ rods, which interact *via* 'secondary' (see below) Bi—S and Bi—Br bonds (Fig. 3). With respect to the Bi$-X$ bond-length changes that the three series undergo when X is varied, they are to be compared with a number of isotypic alkali halide series AX (A = Na, K, Rb and Cs; X = F, Cl, Br and I; Donnay *et al.*, 1963).

In general, structures of Bi^{III} compounds are special cases because of the Bi^{III} lone electron pair (LEP). Any LEP of an atom E^L may show 'stereochemical activity' (*e.g.* Galy *et al.*, 1975; Trömel, 1980), leading, for example, to a grouping of the bonds to E^L into short 'primary' and long 'secondary' bonds

(Alcock, 1972), the latter to be found in the neighbourhood of the LEP. For numerous E^{L} compounds, significant deviations from bond lengths predicted by the classical BV concept are observed, mainly for secondary bonds. Such deviations can be dealt with by *in*creasing the conventional BV b parameter [mostly to values around 0.5 valence units (v.u.)], while concurrently *de*creasing the $R0$ parameter slightly (Wang & Liebau, 1996; Preiser *et al.*, 1999; Krivovichev & Brown, 2001). Too few examples have been published, however, to allow us to judge whether the increased b values for bonds to different isovalent anions are equal (or, at least, very similar). On the other hand, expectation values for ionic size differences – to be used as reference values in this work – have been calculated from classical BV $R0$ parameters under the condition of such an equality (Keller & Krämer, 2006). Therefore, the discussion of our results must take possible effects of the Bi^{III} LEP into account.

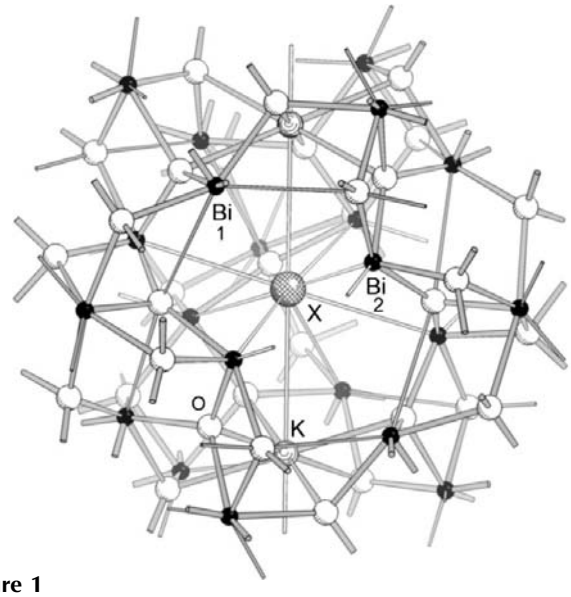

Figure 1
Spherical section of the structure of KBi_6O_9X (X = Br), with X at the centre, as seen from [0$\bar{2}$3]. As in all other figures, secondary bonds (and the K—X bonds) are indicated by sticks of reduced thickness; parts of the structure that are more distant from the viewer have been drawn lighter. For a view of the complete unit cell, see Eggenweiler *et al.* (1998).

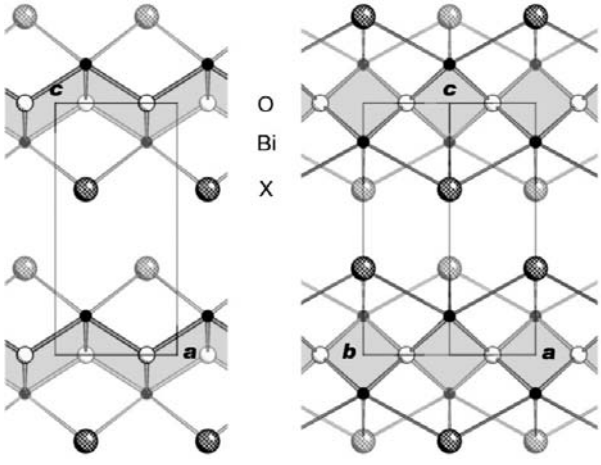

Figure 2
Structure of BiOX (X = Br) as seen from [0$\bar{1}$0] (left) and from [$\bar{1}\bar{1}$0] (right).

2. Results and discussion

In Fig. 4, we have plotted the Bi—X bond-length difference ΔD_{XY} (which is observed when the halogen atom X is replaced by a halogen atom Y of a different kind) for the various series against the calculated X/Y size difference expectation values $\langle\Delta\rho_{XY}\rangle$ (see above) in two different ways. In Fig. 4(a), ΔD_{XY} is plotted directly *versus* $\langle\Delta\rho_{XY}\rangle$. In Fig. 4($b$), $(\Sigma\Delta D_{XY}) - \Delta D_{\mathrm{F\,Cl}}$ is plotted against $(\Sigma\langle\Delta\rho_{XY}\rangle) - \langle\Delta\rho_{\mathrm{F\,Cl}}\rangle$, thus indicating the changes when X is successively replaced by the next larger ion. A plot of $(D_{A-Y} - D_{A-\mathrm{Cl}})$ *versus* $(\mathrm{IR}_Y - \mathrm{IR}_{\mathrm{Cl}})$ would look very similar in this case because $\langle\Delta\rho_{XY}\rangle$ and $\Delta\mathrm{IR}_{XY}$ differ only marginally for the halide ions. In other cases (Keller & Krämer, 2006), the degree of similarity would be lower owing to larger differences between $\langle\Delta\rho_{AB}\rangle$ and $\Delta\mathrm{IR}_{AB}$. While in most of the above series all E—X bonds in the structure are symmetry equivalent, there are two pairs of Bi—X bonds, namely primary and secondary bonds, with very different bond lengths in the BiSX structure; these bonds have been considered separately in Fig. 4.

Not surprisingly, the data points for the series of isotypic alkali halides are close to the (dotted) ideal lines of slope 1 in Fig. 4. The maximal AX difference $|\Delta D_{XY} - \langle\Delta\rho_{XY}\rangle|$ of 0.03 Å (in the NaX series) in Fig. 4(a) can be taken as an approximate measure for a deviation that still can be counted as 'normal'. Accordingly, the secondary Bi—X bonds in the BiSX series with a maximal deviation of 0.02 Å can likewise be classified as 'normal'. There are larger deviations, however, for the primary

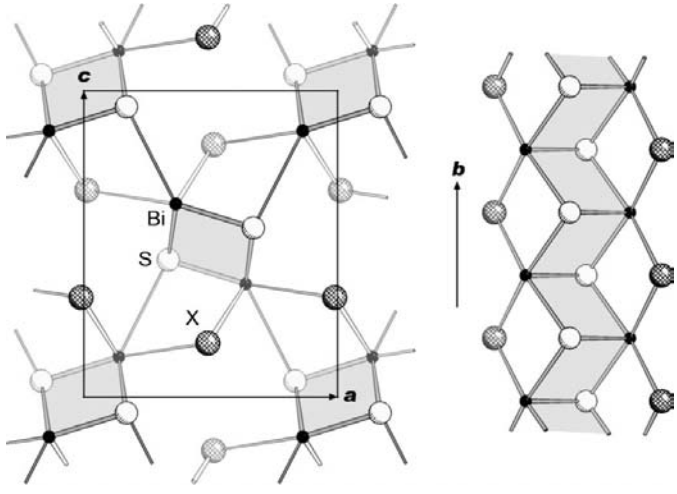

Figure 3
Left: structure of BiSX (X = Br) as seen from [0$\bar{1}$0]. Right: the central $X[Bi_2O_2]X$ rod as seen from [210]; each Br (Bi) atom is bonded by two (three) additional secondary bonds (not shown) to two Bi (2Br + 1S) atoms. Shaded areas denote 'folded ladders'.

bonds in BiSX, and severe deviations for the two isotypic series of bismuth *oxide* halides.

2.1. KBi_6O_9X

In the series KBi_6O_9X, where X is sitting in a void of the $\{^3_\infty\}[Bi_2O_3]$ framework coordinated by six Bi and two K atoms, the experimental ΔD values are far below the expected values. This fact is reflected in the observation that the cubic lattice parameter a grows by only 0.20 Å from X = Cl to X = I (Table 1). An analysis of the connection scheme with *BONDVAL* (Orlov *et al.*, 1998; Orlov & Popov 2002) using 'Pauling weights by cations' provides a simple explanation: the bonds within the $\{^3_\infty\}[Bi_2O_3]$ framework have ideal valences of 0.6–0.7 v.u., while the X–Bi bonds have valences of only about 0.16 v.u. (*i.e.* about 1/4 of the Bi—O valences). If Cl is replaced by Br and then by I, the anion size difference is, in principle, supposed to result in a corresponding elongation of the X—Bi bonds, *i.e.* in an expansion of the X-carrying voids in the $[Bi_2O_3]$ framework. However, the steric strain induced by the new halogen ion *via* its low-valence bonds is too weak to make the strongly bound framework change more than marginally (Fig. 5). Stated the other way around, the steric strain produced by the framework leads to 'wrong' low-valence bond lengths (Brown, 1992) and therefore to 'wrong' experimental anion size differences.

Before this explanation can be taken as sufficient, a possible influence of the Bi^{III} LEP (see above) must also be considered. The Bi—X bonds in KBi_6O_9X (with lengths of about 3.6 Å)

Table 1
Lattice constants a and distances D in KBi_6O_9X (in Å).

Compound	a	D_{Bi-X}	Reference
KBi_6O_9Cl	17.050	3.549	Eggenweiler *et al.* (1998)
KBi_6O_9Br	17.117	3.572	
KBi_6O_9I	17.254	3.620	

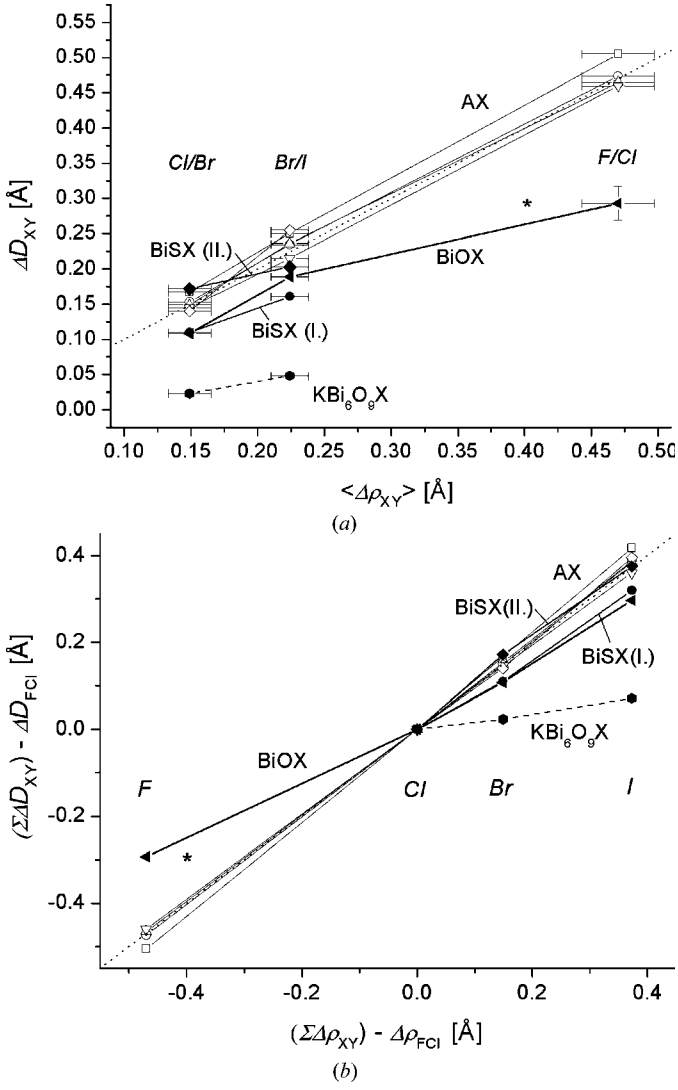

Figure 4
(*a*) Plot of ΔD_{XY} *versus* $\langle\Delta\rho_{XY}\rangle$ for some series of isotypic compounds. The vertical error bar for BiOF is due to the difference between the two published Bi—F bond lengths (Table 2). (*b*) Plot of $(\Sigma\Delta D_{XY}) - \Delta d_{F\,Cl}$ *versus* $(\Sigma\,\langle\Delta\rho_{XY}\rangle) - \langle\Delta\rho_{F\,Cl}\rangle$, where the sums are (from left to right) over one, two, three *etc.* values. Data points plotted in grey represent the NaCl structure series AX (X = F, Cl, Br and I), with A = Na (squares), K (circles), Rb (up-triangles) and Cs (down-triangles), and the CsCl structure series CsX (X = Cl, Br and I) (diamonds). The long dotted straight lines represent the function $f(x) = x$. '(I.)' denotes primary and '(II.)' secondary Bi—X bonds. For the meaning of the data points marked '*', see text.

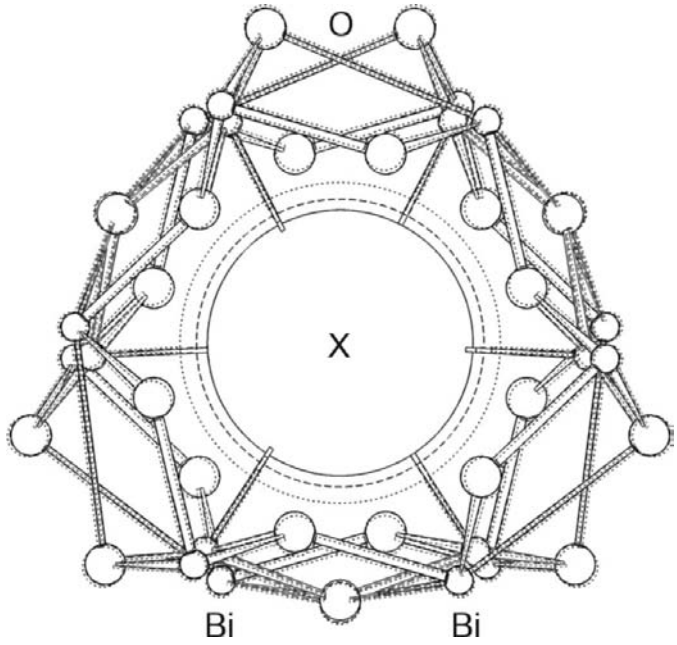

Figure 5
Superposition of analogous sections of the structures of KBi_6O_9X (X = Cl, Br and I); the contents of a cylindrical section of radius 5.3 Å and height 6 Å centred at X (but with K omitted) as seen from [111] are plotted in solid (Cl), dashed (Br) and dotted (I) lines. The radii of the halogen atoms correspond to IR_{Cl} (Cl), $IR_{Cl} + \langle\Delta\rho_{Cl\,Br}\rangle$ (Br) and $IR_{Cl} + \langle\Delta\rho_{Cl\,I}\rangle$ (I), while the radii of the Bi and O atoms correspond to one-fifth of their IR. With respect to most Bi and O atoms, the differences between the X = Cl and X = Br structures are so small that the latter cannot be distinguished visually.

Table 2
Structural parameters of BiOX and PbFX structures; lattice parameters, interatomic distances D and differences Δ between interatomic distances and ionic radii sums are in Å; experimental valences (S) are in v.u.

Compound	a	c	D_{M-X}	S_{M-X}	$D_{(M-X)'}$†	$S_{(M-X)'}$	D_{X-X}	Δ_{X-X}‡	D_{X-E}§	Δ_{X-E}¶	Reference	Method††
BiOF	3.747	6.226	2.75	0.13	2.92	0.08	3.44	0.78	2.75	0.04	Aurivillius (1964)	XSF
	3.756	6.234	2.80	0.11	2.77	0.12	3.27	0.61	2.87	0.16	Soubeyroux *et al.* (1984)	NPD
	3.752	*6.230*	*2.78*	*0.12*	*2.84*	*0.10*	*3.35*	*0.70*	*2.81*	*0.10*	*Average*	
BiOCl	3.892	7.375	3.06	0.21	3.50	0.06	3.49	−0.13	3.26	0.07	Keramidas *et al.* (1993)‡‡	XSD
BiOBr	3.927	8.106	3.17	0.23	4.08	0.02	3.76	−0.16	3.41	0.07	Ketterer & Krämer (1986)‡‡	XSD
BiOI	3.995	9.151	3.36	0.25	4.88	0.00	4.16	−0.24	3.64	0.06	Keller & Krämer (2005)	XSD
PbFCl	4.106	7.226	3.09	0.22	3.20	0.16	3.61	−0.01	3.27	0.15	Kodama *et al.*, 1984	XSD
PbFBr	4.18	7.59	3.19	0.23	3.45	0.11	3.74	−0.18	3.38	0.11	Nieuwenkamp & Bijvoet (1932)	XPF
PbFI	4.237	8.800	3.36	0.21	4.39	0.01	4.15	−0.25	3.64	0.13	Weil & Kubel (2001)	XSD

† 'Bond' across $X-X$ interface. ‡ $D_{X-X} - 2\mathrm{IR}_X$ [IR = ionic radius for CN 6 (Shannon, 1976)]. § E = O (BiOX) or F (PbFX). ¶ $D_{X-\mathrm{O}} - (\mathrm{IR}_X + \mathrm{IR}_\mathrm{O})$ or $D_{X-\mathrm{F}} - (\mathrm{IR}_X + \mathrm{IR}_\mathrm{F})$. †† Method: X = X-ray, N = neutron; S = single crystal, P = powder; D = diffractometer, F = film. ‡‡ Lattice parameters taken from Keller & Krämer (2005).

clearly are secondary bonds (Fig. 6). Can such bonds be expected to grow (or shrink) according to $\langle\Delta\rho_{XY}\rangle$ when X is replaced by Y? To answer this question, we looked for isotypic series of structurally well defined simple binary or ternary halide compounds with secondary bonds and found the two series PbX_2 (X = Cl and Br; Lumbreras *et al.*, 1986) and SbSX (X = Br and I; Siapkas *et al.*, 1986; Lukaszewicz *et al.*, 1997) besides the 'title series' BiSX (X = Cl, Br and I). The tabulated $\langle\Delta\rho_{XY}\rangle$ values for the Cl → Br and Br → I transitions are 0.15 (2) and 0.22 (2) Å, respectively. The lengths of the secondary E^L—Cl bonds grow by 0.19 (5) (Pb—Cl) and 0.17 Å (Bi—Cl), and those of the E^L—Br bonds by 0.20 Å (Sb—Br and Bi—Br). Thus, the answer to the above question 'can the bonds be expected to shrink or grow according to $\langle\Delta\rho_{XY}\rangle$?' is 'yes'. The Bi LEP is therefore probably *not* responsible for the small ΔD_{XY} values observed in KBi_6O_9X.

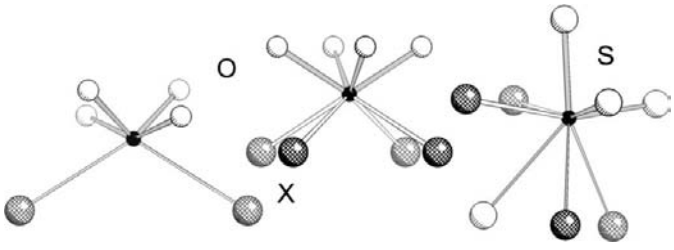

Figure 6
Coordination polyhedra of Bi in KBi_6O_9X (left), BiOX (centre) and BiSX (right). The Bi LEP is supposed to be directed vertically downwards in all three cases. Note that in BiSX the Bi atom participates in *two* secondary bonds to X but only in *one* secondary bond to S.

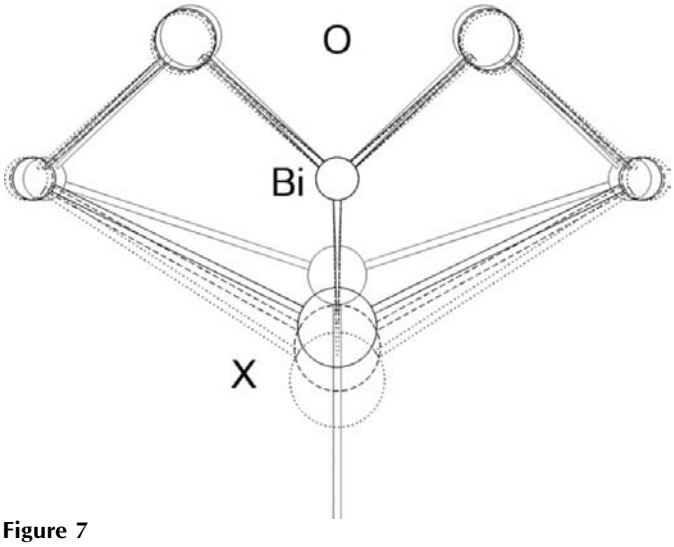

Figure 7
Superposition of analogous sections of the structures of BiOX (X = F, Cl Br and I) as seen from [110]. For BiOF (grey lines), the averaged structure model (Table 2) has been used. For the other three structures, solid (Cl), dashed (Br) and dotted (I) lines have been used.

2.2. BiOX

The distribution of ideal valences between Bi—O (0.5 v.u.) and Bi—X (0.25 v.u., but see below) bonds is similar in the tetragonal BiOX structures (as compared with the KBi_6O_9X structures) but with a valence ratio of only 2 instead of 4. Correspondingly, a (about 4 Å) again undergoes only small changes [Δa = 0.25 Å (0.10 Å) from X = F (Cl) to X = I], but $\Delta a/a$ for the transition Cl → I is about two times as large as that in KBi_6O_9X, owing to the smaller valence ratio. The *absolute* changes in a are nevertheless small, and with only this fact in mind, some of the BiOX data points in Fig. 4(a) are surprisingly *close* to the ideal line. An explanation comes from the observation that c, on the other hand, grows by 2.9 Å in the series F → I. Actually, in this layer structure, a larger halide-ion has the freedom to elongate its bonds to Bi – even if the $\left\{{}^{2}_{\infty}\right\}[Bi_2O_2]^{2+}$ framework does not give way much – by moving in the third dimension (*i.e.* parallel to **c**), as shown in Fig. 7. With respect to BiOX, the calculation of 'ideal' lengths for B—X bonds with ideal valences $s_{\mathrm{Bi}-X}$ = 0.25 v.u. (0.20 v.u. for Bi—F, see below) using classical BV parameters shows that the Bi—I bond is as expected, while the Bi—Br, Bi—Cl and Bi—F bonds are elongated by 0.04, 0.07 and 0.19 Å, respectively. These elongations can be – at least in part – assigned to the Bi LEP, its axis pointing from Bi to the centre of the four X ligands (Andersson & Åström, 1972; Fig. 6). It should be noted, however, that the stereochemical activity of the LEP in BiOX is certainly substantially lower than that in KBi_6O_9X because of the much higher regularity of the coordination

Table 3
Structural parameters of BiSX structures in Å (obtained by single-crystal X-ray diffractometer measurements).

Compound	a	b	c	D_{Bi-X} (I.)†	D_{Bi-X} (II.)‡	D_{Bi-S} (I.)†	D_{Bi-S} (II.)‡	D_{X-X}§	δ_{X-X}¶	Reference
BiSCl	7.751	3.996	9.992	2.927 (2×)	3.367 (2×)	2.605 2.711 (2×)	3.485	4.35	0.86	Voutsas & Rentzeperis (1980)
BiSBr	8.167	4.049	9.853	3.037 (2×)	3.539 (2×)	2.606 2.720 (2×)	3.508	4.01	0.25	Voutsas & Rentzeperis (1984)
BiSI	8.519	4.172	10.177	3.198 (2×)	3.742 (2×)	2.592 2.740 (2×)	3.772	4.03	−0.13	Haase-Wessel (1973)

† Primary bond(s). ‡ Secondary bond(s). § Distance $X^{I}-X^{II}$ (Fig. 8). ¶ D_{X-X}(BiSX) − D_{X-X}(BiOX).

polyhedron (Fig. 6). This fact implies that the Bi—X bonds are primary rather than secondary bonds.

While within the series BiOX (X = Cl, Br and I) the ΔD_{XY} values can be classified as 'rather normal' (Fig. 4), the $\Delta D_{F\,Cl}$ value is much 'too low' as Bi—F is much 'too long'. In principle, F could further shorten its bonds to the four Bi ligands by moving farther towards the centre of the latter (*i.e.* upwards in Fig. 7). However, such a movement is probably inhibited by F—O repulsion (see Δ_{X-E} in Table 2). Anion–anion repulsion may therefore be counted as a second cause for the large deviations from the ideal line in the BiOX series.

In BiOF, the halogenide ion, in complete contrast to the situation in the Br and I structures, is additionally connected to a Bi atom in the vicinal F[Bi_2O_2]F sandwich (see the bond stick pointing vertically downwards in Fig. 7) with a bond of the same 'experimental' valence $S_{(Bi-F)'}$ as that of the other four Bi—F bonds (Table 2). In BiOCl, the fifth bond may be present too, but if so it is very weak, the classical experimental valence $S_{(Bi-Cl)'}$ being only one-quarter to one-third of that of the other four Bi—Cl bonds. In BiOF, the fifth bond, made possible by the comparatively small thickness of the Bi/F/F/Bi quadruple layer, cannot be neglected; it therefore reduces the *ideal* Bi—F valence s_{Bi-F} for the other four Bi—F bonds from 0.25 to 0.20 v.u. This change leads to an increase of the *ideal* Bi—F bond length by b(ln0.25 − ln0.20), *i.e.* 0.08–0.11 Å (for values of b between 0.37 and 0.5 Å). The size-difference expectation value, $\langle\Delta\rho_{F\,Cl}\rangle$, should in this case therefore be reduced by about 0.10 Å or by a little less, say 0.07 Å, accounting for the assumption that in BiOCl a weak fifth bond is also present. Modified F and F/Cl data points (obtained by corresponding $\langle\Delta\rho_{X,Y}\rangle$ shifts) allowing for the changes in the connectivity scheme are included in Fig. 4 (symbol *).

A remarkable feature of the BiOF structure is the $X-X$ distance of 3.35 (8) Å, which is – in sharp contrast to the three other structures (plus some related ones; see Δ_{X-X} in Table 2) – much larger than the sum of the ionic radii (2.66 Å) or the sum of the van der Waals radii (2.8 Å). A reduction of the $X-X$ distance clearly would yield van der Waals energy. The reason that this does not happen can be found in the Bi atom's LEP (see above), which is directed exactly towards the fifth F ligand and presumably prevents it from moving closer to Bi and – as a consequence – closer to the four other F atoms bonded to Bi.

Another question arises with respect to the fifth Bi—F bond, namely, whether BiOF can actually be called 'isotypic' to BiOBr and BiOI despite the different connectivity scheme. As already mentioned, all four BiOX structures are said to belong to the PbFCl (matlockite) structure type [for example, in the ICSD (FIZ Karlsruhe)] or to one of its two subtypes, the BiOCl type (Flahaut, 1974). In the PbFCl structure (Kodama *et al.*, 1984) itself, Cl is five-coordinated, as is F in BiOF, while in the 'isotypic' PbFI structure (Weil & Kubel, 2001) the fifth bond is missing, as it is in BiOBr and BiOI; PbFBr – as far as its structure determination by powder film methods (Nieuwenkamp & Bijvoet, 1932) allows us to judge – is once more an intermediate case. If the term 'isotypic' and related terms (Lima-de-Faria *et al.*, 1990) could have been defined *strictly*, BiOF and PbFCl could not even be classified *isoconfigurational* to BiOBr, BiOI and PbFI. As things are, however, the term 'isotypic' can be retained for all these compounds, provided that the coordination of X in the two kinds of species (four- and five-coordinated) are judged to be 'similar'. The observation that in both series the transition from one species to the other is smoothed by an intermediate clearly supports this judgement. In any case, the BiOX series teaches that the comparison of experimental and expected 'ionic' size differences in 'isotypic' series generally should include a check of the integrity of the connectivity scheme.

2.3. BiSX

It should be noted that the BiSCl structure has been described with the conventionally set space group *Pnma* (Voutsas & Rentzeperis, 1980), while the BiSBr and BiSI structures were solved in the space group *Pnam* (Voutsas & Rentzeperis, 1984; Haase-Wessel, 1973). In the following, all axis names refer to the *Pnma* setting. The corresponding rearrangement of the lattice parameters (Table 3) reveals that, while a and b grow as expected in the series Cl → I, c is minimal for BiSBr, an anomaly that requires explanation. As already mentioned above, the BiSX structure consists of parallel $\{^{1}_{\infty}\}[X(Bi_2S_2)X]$ 'rods' with their axes parallel **b**, and these rods interact *via* secondary Bi—S and Bi—X bonds; their cores are folded $\{^{1}_{\infty}\}[Bi_2S_2]^{2+}$ 'ladders' (Fig. 3). In the **b** direction, the structure expands only slightly in the series Cl → I (by 0.17 Å, $\Delta b/b$ being about 1.5 times as large as for BiOX), and again this lack of expansion can be understood by the stronger ideal valence s_{Bi-S} [0.5 (0.67) v.u.] as compared with s_{Bi-X} [0.25 (0.5) v.u.], secondary bonds (not) accounted for in the connectivity scheme. As in BiOX, the X atoms are nevertheless able to approximate the expected size differences by moving in the 'third dimension', *i.e.* in directions perpen-

dicular to the lines defined by the two Bi atoms they are bonded to by primary bonds and the two they are bonded to by secondary bonds (Figs. 3 and 8).

In Fig. 8, parts of the three BiS*X* structures are superimposed, such that the 'folded ladders' in the centres of the unit cells coincide. Obviously, the structural changes caused by the Cl → Br → I transitions are more complex than in the previous two series. The structural rearrangements and the *c* anomaly mentioned above can be explained by the formulation of two sequences of (occasionally slightly simplified) fictional steps, the first sequence to take place after the substitution of all Cl atoms in BiSCl by Br atoms (Cl and Br positions initially coinciding):

(1) To elongate its primary bond to Bi and concurrently increase the distance to S^{I}, Br^{I} moves towards Br^{II}, *i.e.* approximately parallel to +**c**. As it happens, there is 'unused' space available in this direction owing to a 0.8 Å gap between Cl^{I} and Cl^{II} (δ_{X-X} in Table 3). Rod '*B*' (Fig. 8) is shifted along, leading to a temporary increase of *c*. As required by symmetry, Br^{II} and Br^{III} move into 'their' gaps in the opposite direction; thus, the corresponding elongation of the primary bond between Br^{III} and rod *A* does *not* cause a shift of the latter in the +**c** direction.

(2) To elongate its secondary bond to Bi, Br^{I} shifts rod *B* parallel to +**a**. For the same reason, Br^{III} pushes itself and the rod labelled *A* parallel to –**a**. Both shifts together lead to a significant increase of *a*. All movements add to those of step 1.

(3) Steps (1) and (2) have led to an undesired elongation of the secondary Bi—S bonds. To readjust them (approximately) to their former length, rods *A* and *B* rotate clockwise by *ca* 4° about two [010] axes, the first located at Br^{III} and the second at Br^{I}. These rotations are provoked by the residual gap between Br^{I} and Br^{II} (and its copy in the vicinal unit cell) but do not close it completely, the final Br—Br distance still being 0.25 Å longer than that in BiOBr (where it can adjust itself free from external forces) (see δ_{X-X} in Table 3).

(4) The clockwise rotation of *A* more or less *compensates* the *A* shift of step 2, while the rotation of *B enhances* the *B* shift of step 2 (the increase of *a* being, from this point of view, only generated by rod *B*). Furthermore, owing to the relative positions of the two rotation axes, the rotation of *B over*-compensates the *in*crease of *c* in step 1 (leading to a net *c* *de*crease), while the centre of *A* hardly moves in the **c** direction. As a consequence of both mechanisms, the unit-cell edges rotate by 1.5° clockwise. Orthogonality, temporarily abandoned in step 1, is reestablished owing to the desire to retain the high orthorhombic symmetry.

In summary, the decrease of *c* (as compared with BiSCl) seems to be caused mainly by the tenacity of the secondary Bi—S bond, and it is made possible by the gap between Cl^{I} and Cl^{II}. The second of the two sequences of steps takes place after the (initially coincidental) replacement of Br by I. Note that the residual gap between Br^{I} and Br^{II} (step 3) vanishes completely by this replacement owing to the larger radii (by more than 0.2 Å) of the two I atoms.

(5) To elongate its primary bond to Bi, I^{I} moves towards I^{II}. As the *X*—*X* gap has disappeared, this movement (and the corresponding elongation of the primary bond between I^{III} and rod *A*) must push I^{II} and rods *A and B* 'upwards' (in Fig. 8), leading to a significant increase of *c*. The desire to reduce I^{I}–I^{II} repulsion adds a second shift in the same direction.

(6) To elongate their secondary bonds to Bi, I^{I} and I^{III} behave like Br^{I} and Br^{III} in step 2, pushing rods *A* and *B* 'outwards' (parallel to −**a** and +**a**).

(7) Once more, the combination of steps (5) and (6) forces an elongation $\Delta D_{\mathrm{Bi-S(II.)}}$ of the secondary Bi—S bond. To reduce it, rods *A* and *B* do their best in rotating clockwise (for rod *B*, the rotation axis moves to the rod axis; for rod *A*, it is a shift rather than a rotation). They manage only *ca* 1°, as the gap between I^{I} and I^{II} is more than closed at this point, the final δ_{X-X} (Table 3) being negative (−0.13 Å). On the other hand, the operation is, by far, insufficient, the whole procedure ending in a $\Delta D_{\mathrm{Bi-S(II.)}}$ of +0.16 Å, which can be seen as a 'counterweight' to the aforesaid I–I 'compression' of 0.13 Å and to the 'too small' increase of the Bi—*X* bond lengths (see below).

(8) By mechanisms similar to those described for step 4, the unit-cell edges again rotate clockwise, but – almost negligibly – only by about 0.5° this time.

This explanation leaves the question of why the secondary Bi—*X* bonds are more successful in adjusting expected *X* size differences than are the primary bonds (Fig. 4). One reason can be found in the directions of the secondary Bi—S bonds, which make angles of less than 30° to the direction of movements necessary to adjust the *primary* Bi—*X* bond length, and angles greater than 50° to the direction of movements to adjust the *secondary* Bi—*X* bond length. The corresponding binding forces – which are the only forces that can play a role at all in this context – should therefore be able to provide

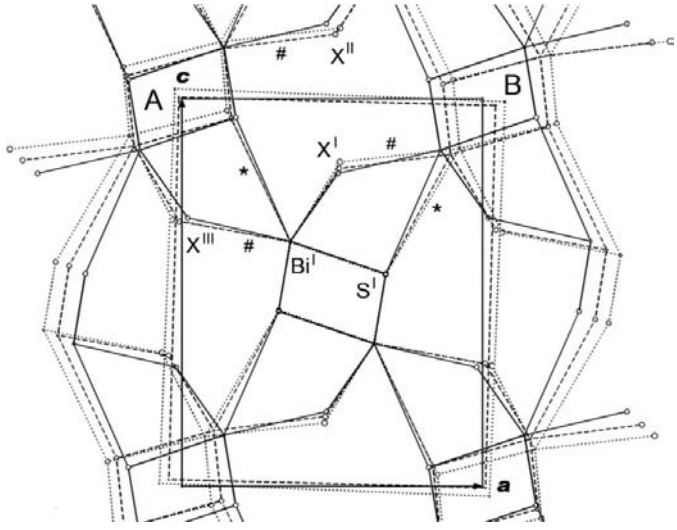

Figure 8
Superposition of the three structures of BiS*X* [*X* = Cl (solid), Br (dashed) and I (dotted lines)] as seen from [010]. Secondary Bi—*X* bonds are flagged by '#' and secondary Bi—S bonds by '*' (see also Fig. 6).

more resistance against the elongation of the primary bonds compared with the secondary ones.

The comparatively small slope of the line connecting the two data points for the secondary bonds in Fig. 4(*a*) suggests that – at least for the Br → I transition – these bonds nevertheless experience resistance as well.

3. Conclusion

Owing to their low *atomic* valence, halide ions (like alkali metal ions) are usually bound by low-valence *bonds* in solid-state chemistry. Therefore, if higher-valent bonds are also present in a structure, the structure-determining power of such ions is comparatively low (Brown, 1992). Nevertheless, the BiO*X* and BiS*X* series discussed above demonstrate that it is possible for halide ions to (nearly) adjust expected isotypic size differences, even if the low-valence bonds are embedded in a framework of higher-valence bonds. On the other hand, it is also possible for experimental size differences to (nearly) vanish, if this framework is three-dimensionally infinite, as is the case in KBi_6O_9X.

References

Alcock, N. W. (1972). *Adv. Inorg. Radiat. Chem.* **15**, 1–57.

Andersson, S. & Åström, A. (1972). National Bureau of Standards, Special Publication 364, Solid-State Chemistry. Proc. of 5th Materials Research Symposium. Issued July 1972.

Aurivillius, B. (1964). *Acta Chem. Scand.* **18**, 1823–1830.

Brown, I. D. (1992). *Acta Cryst.* B**48**, 553–572.

Donnay, J. H., Donnay, G., Cox, E. G., Kennard, O. & King, M. V. (1963). *Crystal Data Determinative Tables*, 2nd ed. American Crystallographic Association.

Eggenweiler, U., Keller, E. & Krämer, V. (1998). *Z. Kristallogr.* **213**, 377–381.

Flahaut, J. (1974). *J. Solid State Chem.* **9**, 124–131.

Galy, J., Meunier, G., Andersson, S. & Aström, A. (1975). *J. Solid State Chem.* **13**, 142–159.

Haase-Wessel, W. (1973). *Naturwissenschaften*, **60**, 474.

Keller, E. & Krämer, V. (2005). *Z. Naturforsch. Teil B*, **60**, 1255–1263.

Keller, E. & Krämer, V. (2006). *Acta Cryst.* B**62**, 411–416.

Keramidas, K. G., Voutsas, G. P. & Rentzeperis, P. I. (1993). *Z. Kristallogr.* **205**, 35–40.

Ketterer, J. & Krämer, V. (1986). *Acta Cryst.* C**42**, 1098–1099.

Kodama, N., Tanaka, K., Marumo, F., Utsunomiya, T. & Hoshino, Y. (1984). *Kobutsugaku Zasshi* (*J. Min. Soc. Jpn*), **16**, 309–316.

Krivovichev, S. V. & Brown, I. D. (2001). *Z. Kristallogr.* **216**, 245–247.

Lima-de-Faria, J., Hellner, E., Liebau, F., Makovicky, E. & Parthé, E. (1990). *Acta Cryst.* A**46**, 1–11.

Lukaszewicz, K., Pietraszko, A., Stepien-Damm, J. & Kajokas, A. (1997). *Pol. J. Chem.* **71**, 1852–1857.

Lumbreras, M., Protas, J., Jebbari, S., Dirksen, G. J. & Schoonman, J. (1986). *Solid State Ion.* **20**, 295–304.

Nieuwenkamp, W. & Bijvoet, J. M. (1932). *Z. Kristallogr.* **81**, 157–160.

Orlov, I. P. & Popov, K. A. (2002). *BONDVAL.* Version 2.01. Laboratoire de Cristallographie, EPFL, Lausanne, Switzerland. Current version can be downloaded from http://orlov.ch/bondval/.

Orlov, I. P., Popov, K. A. & Urusov, V. S. (1998). *J. Struct. Chem.* **39**, 575–579.

Preiser, C., Lösel, J., Brown, I. D., Kunz, M. & Skowron, A. (1999). *Acta Cryst.* B**55**, 698–711.

Shannon, R. D. (1976). *Acta Cryst.* A**32**, 751–767.

Siapkas, D., Bartzokas, A., Voutsas, G. P. & Rentzeperis, P. J. (1986). *Z. Kristallogr.* **175**, 305–315.

Soubeyroux, J. L., Matar, S. F., Reau, J. M. & Hagenmuller, P. (1984). *Solid State Ion.* **14**, 337–345.

Trömel, M. (1980). *J. Solid State Chem.* **35**, 90–98.

Voutsas, G. P. & Rentzeperis, P. J. (1980). *Z. Kristallogr.* **152**, 109–118.

Voutsas, G. P. & Rentzeperis, P. J. (1984). *Z. Kristallogr.* **166**, 153–158.

Wang, X. & Liebau, F. (1996). *Acta Cryst.* B**52**, 7–15.

Weil, M. & Kubel, F. (2001). *Acta Cryst.* E**57**, i80–i81.